The Influence of Cytotoxicity of Macromolecules and of *VEGF* Gene Modulated Vascular Permeability on the Enhanced Permeability and Retention Effect in Resistant Solid Tumors

Tamara Minko,[1] Pavla Kopečkova,[1,2] Vitaliy Pozharov,[3] Keith D. Jensen,[1] and Jindřich Kopeček[1,2,4]

Received November 16, 1999; accepted January 28, 2000

Purpose. To study the influence of cytotoxicity of macromolecules, *VEGF* gene expression, and vascular permeability on the enhanced permeability and retention (EPR) effect.

Methods. Mice bearing xenografts of A2780 multidrug resistant human ovarian carcinoma were treated by free doxorubicin (DOX) and N-(2-hydroxypropyl)methacrylamide (HPMA) copolymer-bound DOX (P(GFLG)-DOX), Texas Red (P-TR), and FITC (P-FITC). Antitumor activity, drug distribution in tumor, vascular permeability, *VEGF* gene expression, and DNA fragmentation were studied.

Results. The accumulation of free DOX led to the *VEGF* gene overexpression and increased the vascular permeability, which in turn enhanced the drug accumulation in the same location. This positive feedback loop led to a highly inhomogeneous distribution of the drug within the tumor. In contrast, P(GFLG)-DOX down-regulated the *VEGF* gene and decreased vascular permeability. This negative feedback seemed to prevent additional drug accumulation in dead necrotic tissue, resulting in a more uniform drug distribution and enhanced the antitumor activity P(GFLG)-DOX.

Conclusions. The EPR effect significantly differed for macromolecules containing DOX when compared to macromolecules without drug. The cytotoxicity of P(GFLG)-DOX amplified the EPR effect, led to a more homogenous distribution of the drug, increased the average drug concentration in tumor and augmented its efficacy.

KEY WORDS: HPMA copolymer; enhanced permeability and retention effect; *VEGF* gene; antitumor activity; necrosis; doxorubicin.

INTRODUCTION

In our previous *in vitro* (1–3) and *in vivo* (4) studies we found that HPMA copolymer-bound doxorubicin (P(GFLG)-DOX) demonstrated a higher anticancer activity when compared to free doxorubicin (DOX) especially in DOX resistant cells or tumors. We revealed that this phenomenon *in vitro* was the result of the higher intracellular toxicity of P(GFLG)-DOX when compared to free DOX (3). Being internalized in membrane-limited organelles, HPMA copolymer-bound DOX was protected from the cellular drug efflux and detoxification mechanisms, and preserved its activity during intracellular trafficking. As a result, it activated apoptosis and necrosis signaling pathways more significantly than free DOX, and simultaneously inhibited cellular defensive systems. In contrast, free drug activated the defense mechanisms (3). These specific properties of P(GFLG)-DOX were confirmed in an animal model of solid tumor (4). However, the antitumor activity of HPMA copolymer-bound DOX *in vivo* was significantly higher than expected based on the *in vitro* experiments, especially in case of the DOX resistant tumors. We hypothesized that this phenomenon could be explained by the so-called enhanced permeability and retention (EPR) effect, which results in preferential accumulation of macromolecules in solid tumors (5–7). The EPR effect is the result of the increased permeability of the tumor vascular endothelium to circulating macromolecules combined with limited lymphatic drainage from the tumor interstitium. Based on our recent data (4), we hypothesize that the EPR effect for macromolecules containing cytotoxic drugs might significantly differ from macromolecules without drug. The aim of the present study was to verify this hypothesis and investigate the perculiarities and mechanisms of the EPR effect for macromolecules coupled with a cytotoxic drug in an animal model of solid human ovarian tumor resistant to doxorubicin.

MATERIAL AND METHODS

Drug and HPMA Copolymer Conjugates

Doxorubicin was obtained from Dr. A. Suarato, Pharmacia-Upjohn, Milano, Italy.

HPMA copolymer-bound doxorubicin, (P(GFLG)-DOX; P is the HPMA copolymer backbone) was synthesized as previously described (8,9). DOX was attached to the polymer via the lysosomally degradable glycylphenylalanylleucylglycine (GFLG) spacer. Briefly, the conjugate was synthesized using a two step procedure. In the first step, the polymer precursor was prepared by radical precipitation copolymerization of HPMA and N-methacryloylglycylphenylalanylleucylglycine p-nitrophenyl ester. The polymer precursor contained 4.9 mol% active ester groups (M_w = 24000, M_w/M_n = 1.4; aminolyzed polymer; weight average molecular weight, M_w, and polydispersity, M_w/M_n, of polymer were estimated by size exclusion chromatography using the FPLC system, Superose 12 column, buffer PBS, and laser light scattering detector, MiniDawn, Wyatt, Santa Barbara). DOX was bound to the polymer precursor by aminolysis. The conjugate was purified on a Sephadex LH 20 (Pharmacia) column using methanol containing 10% DMSO and 1% CH_3COOH as eluent. The P(GFLG)-DOX conjugate contained 6.3 wt.% (0.117 mmol/g) of DOX (2.0 mol% of DOX containing side-chains) (Scheme 1).

HPMA copolymer bound FITC (P-FITC) was synthesized by copolymerization of HPMA, N-methacryloylglycylglycyl p-nitrophenyl ester and fluorescein containing monomer (5-[-3-(methacryloylaminopropyl)thioureidyl] fluorescein; (10) in the

[1] Department of Pharmaceutics and Pharmaceutical Chemistry, University of Utah, Salt Lake City, Utah.
[2] Department of Bioengineering, University of Utah, Salt Lake City, Utah.
[3] Olympus Research, Salt Lake City, Utah.
[4] To whom correspondence should be addressed. (e-mail: jindrich.kopecek@m.cc.utah.edu)

ABBREVIATIONS: DOX, doxorubucin (adriamycin); HPMA, N-(2-hydroxypropyl)methacrylamide; P(GFLG)-DOX, HPMA copolymer-bound DOX (P is the HPMA copolymer backbone, GFLG, the lysosomally degradable glycylphenylalanylleucylglycine spacer); VEGF, vascular endothelial growth factor/vascular permeability factor; EPR, enhanced permeability and retention; FITC, fluorescein isothiocyanate; TR, Texas Red; P-FITC, HPMA copolymer-bound FITC; P-TR, HPMA copolymer-bound TR.

0724-8741/00/0500-0505$18.00/0

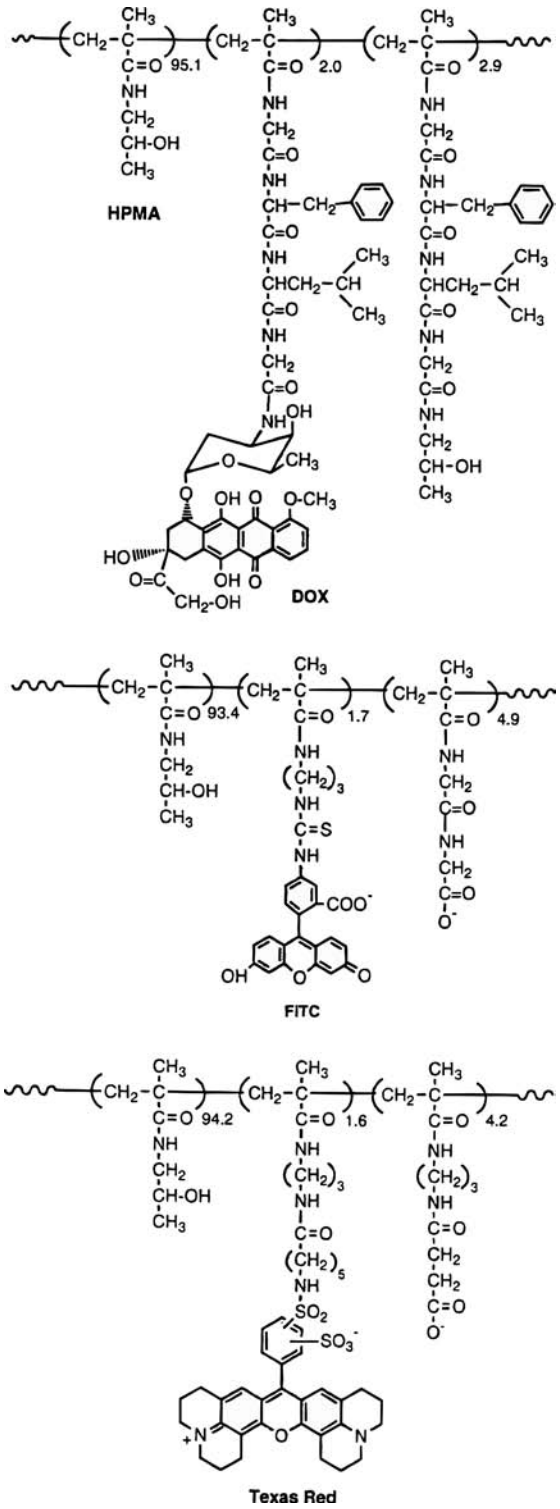

Schematic 1. Structures of HPMA copolymer conjugates.

molar ratio 93:5:2, by radical precipitation polymerization in acetone, with AIBN as the initiator, at 50°C, for 24 h. The reactive p-nitrophenyl ester groups in the resulting polymer were hydrolyzed with NaOH and the polymer was isolated after dialysis (M_w cut off 6–8 kDa) by freeze drying (M_w = 25000, M_w/M_n = 1.5; hydrolyzed polymer). The polymer (Scheme 1) contained 1.7 mol% of FITC containing side-chains (0.112 mmol FITC/g; determined spectrophotometrically, ε = 81000 M^{-1} cm^{-1}, 495 nm, pH 9.2).

HPMA copolymer bound Texas Red (P-TR) was synthesized by a two-steps procedure. First, a polymer precursor was prepared by a copolymerization of HPMA, N-(3-aminopropyl)-methacrylamide hydrochloride, in the presence of 3-mercaptopropionic acid (chain transfer agent); (molar ratio 95:5:0.5) in methanol (10 wt.% monomers), 3 mM AIBN, at 50°C, for 24 h. The polymer was isolated by precipitation into ether, then extensively dialysed (M_w cut off 6–8 kDa) and freeze dried. The polymer contained 5.4 mol% of the amine containing side-chains (M_w = 28000; M_w:M_n = 1.4). In the second step, the Texas Red fluorophore was bound to the amine containing polymer by reacting 100 mg polymer (0.040 mmol NH_2 groups) in 0.8 ml DMSO with 10 mg (0.012 mmol) of Texas Red succinimidyl ester (mixed isomers Molecular Probes T-6134) followed by the addition of 8.4 mg (0.083 mmol) triethylamine (diluted in DMF 1:1). The reaction was stirred for 3 h at room temperature, after that the residual amino groups were reacted with an excess of succinic anhydride (50 mg), followed by the addition of 20 mg triethylamine. The polymer was purified first on a Sephadex LH-20 column in MeOH, then by extensive dialysis (M_w cut off 6–8 kDa). The freeze-dried product contained 1.6 mol% Texas Red containing side-chains (0.099 mmol TR/g; determined spectrophotometrically, ε = 116000 M^{-1} cm^{-1}, 585 nm, MeOH).

Concentration of P(GFLG)-DOX was expressed in DOX equivalents. All solutions were sterilized by filtering through a 0.2-μm filter prior to use.

Cell Line

The DOX resistant human ovarian carcinoma A2780/AD cell line was obtained from Dr. T. C. Hamilton (Fox Chase Cancer Center). Cells were cultured in RPMI 1640 medium (Sigma) supplemented with 10% fetal bovine serum (HyClone) and 10 μg/ml insulin (HyClone). Cells were grown at 37°C in a humidified atmosphere of 5% CO_2 (v/v) in air.

Animal Model of Solid Tumor, Treatment, and Antitumor Activity

The human ovarian carcinoma A2780/AD DOX resistant cells (5×10^6) were subcutaneously transplanted into the flanks of female athymic nu/nu mice. When the tumors reached a size of about 1 cm^2 (13–17 days after inoculation), mice were treated intraperitoneally 6 times over 3 weeks (1st and 4th day of each week) with the maximum tolerated dose of free DOX (5 mg/kg) and P(GFLG)-DOX (25 mg DOX equivalent/kg). These maximum tolerated doses of drugs were estimated in preliminary experiments on tumor bearing mice. P-FITC and P-TR were injected in doses equivalent to the total amount of P(GFLG)-DOX used per mouse. A suppression of tumor growth was used as an indicator of antitumor activity of free DOX and P(GFLG)-DOX. Tumor mass was measured after sacrificing the animals on days 18, 25 and 32.

Drug Distribution in the Tumor

To analyze the distribution of free DOX, P(GFLG)-DOX, P-FITC, and P-TR, tumors and organs (brain, liver, heart, lung,

spleen and kidney) were washed in ice-cold saline and kept frozen. The fluorescent substances were visualized by fluorescence microscopy (Eclipse E800, Nikon) on frozen 5 μm tissue sections using the following filters: "FITC" (excitation: 465–495 nm, emission: 515–555 nm), "TRITC": (excitation: 527–552 nm, emission: 577–632 nm), and "Texas Red": (excitation: 532–587 nm, emission: 607–682 nm) for FITC, DOX, and TR, respectively. The microphotographs were stored in the computer and were processed using original computer programs written by the authors as follows. The fluorescent intensity of each pixel of the microphotograph (3–4 $\times$ 10^5 pixels per photo) was analyzed separately and expressed in relative units (0–255 units scale). The mean intensity of background (spontaneous fluorescence of picture regions, which do not contain tumor tissue) was calculated for the whole picture and subtracted. For individual analysis of the distribution of the fluorophor within the picture the average intensity of 10 adjacent pixels was plotted on ordinate of a 3-dimensional histogram for each picture. The distribution of the fluorescent substances within whole tumor were studied using 10 frozen 5 μm sections of the tumor, which were taken uniformly from the larger diameter of the tumor. Three photographs were made randomly from exterior, medium and central core parts of each section. After measuring the fluorescence intensity of each pixel on each image as described, the histogram of the distribution was made using 10 equal intervals of 25 arbitrary units of fluorescence. Based on these measurement, the average value (M), standard deviation (SD) and coefficient of variation (CV, 100*SD/M) of fluorescence intensity were calculated for each distribution.

Vascular Permeability and *VEGF* Gene Expression

Vascular permeability in tumors and surrounding normal tissue (control) was measured by the accumulation of the albumin-Evans blue complex (5). For the analysis of *VEGF* gene expression total cellular RNA was isolated using RNeasy kit (Qiagen) and QIAshredder micro spin homogenizer (Qiagen). First-strand cDNA was synthesized by Ready-To-Go You-Prime First-Strand Beads (Pharmacia) according to manufacturer instructions with 2 μg of total cellular RNA and 100 ng of random hexadeoxynucleotide primer (Pharmacia). The β_2-microglobulin (β_2-*m*) mRNA was used as an internal standard. PCR was carried out using an Air Thermocycler (Idaho Technology) with the diluted first-strand reaction mixture, 1 unit of Taq Polymerase (GibcoBRL), 0.5 μM of specific primers in a final volume of 50 μl. Primer sequences (11) were GCCAAGCTTGAGTGTGTGCCCACTGAGGAGTCCAACATCACCATGCAG (sense strand) and GCCAAGCTTGCTCCTGCCCGGCTCACCGCCTCGGCTTGTCACA (antisense strand). The positions of the primers and expected size of RT-PCR products are shown in Fig. 1. The PCR regimen was: 94°C/4 min, 55°C/1 min, 72°C/1 min for 1 cycle; 94°C/1min, 55°C/50 sec, 72°C/1 min for 28 cycles, 60°C for 10 min. Agarose gel electrophoresis was used for the separation of PCR products by submarine electrophoresis using MetaPhor agarose (FMC Bio Products) at 4% w/v concentration in 0.5 $\times$ TBE buffer (0.0445 M Tris/Borate, 0.001 M EDTA, pH 8.3; Research Organics Inc.). The gels were stained with ethidium bromide and photographed using a digital camera connected to the computer.

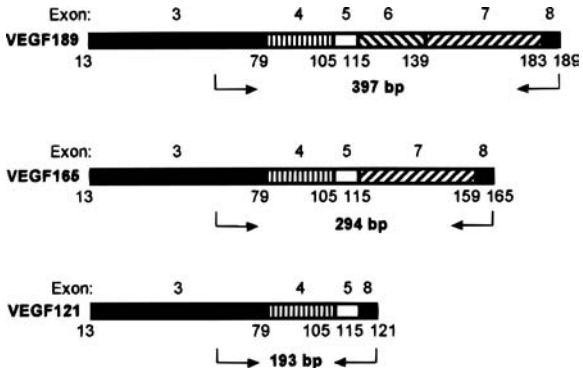

Fig. 1. Primers for detection of the isoforms of VEGF mRNA. Arrows indicate the sites of primers. PCR with primers should give VEGF189 (397 bp), VEGF165 (294 bp) and VGF121 (193 bp) fragments.

Histological Examination, Apoptosis, and Necrosis Detection

Histological examination of tumor and organs was performed after hematoxylin-eosin staining of samples. Two methods were used for the detection of apoptosis in tumor tissue. The first method was based on the measurement of the enrichment of the tissue by mono- and oligonucleosomes using cell death detection ELISA kit (Boehringer) according to the manufacturer recommendations. The second method of apoptosis detection was based on the registration of DNA fragmentation using agarose gel electrophoresis of genomic DNA. Ladder-type DNA digestion pattern was considered as an index of apoptosis, while random digestion was used as an indication of necrosis (12). DNA was isolated and purified using a commercial kit (Qiagen).

Statistics

The difference between variants was considered significant if $P < 0.05$, determined by single factor analysis of variance (ANOVA).

RESULTS

Antitumor Activity

The antitumor activity of the drugs was estimated by measuring of the tumor mass and size after 18, 25, and 32 days of treatment. It was found that P-FITC and P-TR did not produce any significant changes in the tumor mass and size (Fig. 2). Free DOX slightly (about 16%) decreased the tumor mass only on 25th day of the experiment and did not change significantly the tumor size. In contrast, P(GFLG)-DOX was highly effective in all analyzed time intervals of the treatment. The antitumor effect of HPMA copolymer-bound DOX was significantly greater when compared to free DOX and increased with the time of incubation. Indeed, P(GFLG)-DOX decreased tumor mass and size to 50% and 31% on the 18th day of the experiment, to 23% and 6% on the 25th day, and to 14% and 6% on the 32nd day, respectively, when compared to control tumor. It appears that at the end of treatment, P(GFLG)-DOX was up to 7 times more effective than free DOX.

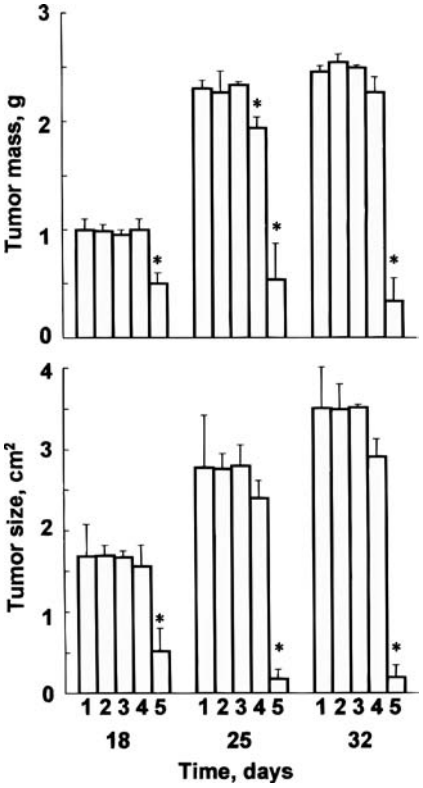

Fig. 2. Changes in the tumor mass and size from untreated animals (1, control) and animals treated by P-FITC (2), P-TR (3) conjugates, free DOX (4), and P(GFLG)-DOX (5). On 18th, 25th and 32nd days of the experiment 3 mice from each series of the experiment were sacrificed and tumor mass was measured. Tumor size at each point was measured in 3–9 animals. Means + SD are shown. * $P < 0.05$ when compared with control.

Drug Distribution

Using fluorescence microscopy of frozen tissue sections, we studied the distribution of labeled HPMA copolymer conjugates in different organs as well as within the tumor. As expected only traces of P-FITC, P-TR, or P(GFLG)-DOX were found in liver, lung, spleen, heart, and kidney (data not shown). All conjugates accumulated preferentially in tumors. Present data support our previous finding (4) that, in addition to the tumor, free DOX accumulated in the liver, kidney, lung, spleen and heart, where its fluorescence was at least twice more pronounced than in the tumor. Detailed analysis of the distribution of the substances within the tumor showed some very important patterns (Figs. 3 and 4). The distribution of free DOX was highly inhomogeneous and demonstrated peaks of the concentration (fluorescence) on the relatively low background. While the distribution of P-FITC and P-TR was more homogeneous, the tendency to form peaks of concentration on the background of a low average concentration was also preserved in these cases. We could not compare the absolute values of fluorescence in these three cases because of the different origin of fluorescent substances (FITC, TR and DOX). However, the comparison of the distribution shape and coefficients of variation revealed some interesting common features. All distributions were asymmetric and shifted to low values of concentrations (Fig. 4). This seems to indicate that the average concentrations of free DOX, P-FITC and P-TR were relatively low. In addition, the concentration fluctuation was very high, the coefficient of variation varied from 60 to 70% in all cases. In contrast, the distribution of P(GFLG)-DOX was more homogeneous and the shape of the distribution was very close to the Gaussian distribution. Although the coefficient of variation in this case was still high (45.6%), it was 1.4–1.5-fold less when compared to free DOX and to conjugates without the cytotoxic drug. In addition, the mean value of fluorescence of HPMA copolymer-bound DOX calculated for the whole tumor was 3.8-times higher when compared to free DOX.

Tumor Morphology

The above mentioned peculiarities of the distribution of free DOX, P-FITC, P-TR and P(GFLG)-DOX may be explained by the EPR effect, which in turn depends on the specifics of tumor morphology. The first determinant, which causes preferential accumulation of macromolecules in solid tumors and inhomogeneous distribution of drugs within the tumor, are the irregularities in tumor blood flow (13). We as well as others (14,15) found numerous blind ends, occlusions, and defects of walls even in the control tumor blood vessels (Fig. 5A, B). Free DOX did not change significantly tumor morphology and the architecture of blood vessels (Fig. 5C, D). In some cases we observed blood vessels with signs of disintegration, uncovered immature and defected vessel walls (Fig. 5D). Treatment with P-TR (Fig. 5E, F) and P-FITC (data not shown) did not produce significant changes in the tumor morphology. In contrast, P(GFLG)-DOX dramatically changed tumor tissues and blood vessels in particular (Fig. 5G, H). The tissue appeared to be necrotic, blood vessels contained frequently thrombi and invasions, and blood flow seemed to be highly limited.

Vascular Permeability

Another feature of the EPR effect is the high permeability of tumor blood vessels (5). To analyze the influence of different treatment protocols we studied the vascular permeability in exterior, intermediate and central core parts of the tumor using Evans Blue accumulation (Fig. 6A, B, D). A much higher permeability of tumor blood vessels when compared to surrounding tissues was observed when analyzing the whole tumor (data not shown) in accordance with our previous data (4) as well as data obtained by other investigators (6). Analysis of the permeability in different parts of tumor showed the following. As expected, the permeability was the highest in the highly vascularized and growing exterior part of the tumor and decreased with increase in tissue depth (Fig. 6D). P-FITC and P-TR did not change significantly tumor vascular permeability (data not shown). Free DOX increased the vascular permeability of the tumor, especially in the exterior and intermediate parts. In contrast, HPMA copolymer-bound DOX produced only a slight increase in the permeability restricted to the exterior parts of the tumor. At the same time, it significantly decreased the permeability inside the tumor.

VEGF Gene Expression

Vascular growth and vascular permeability in the tumor mainly depend on the expression of the *VEGF* gene (16). To

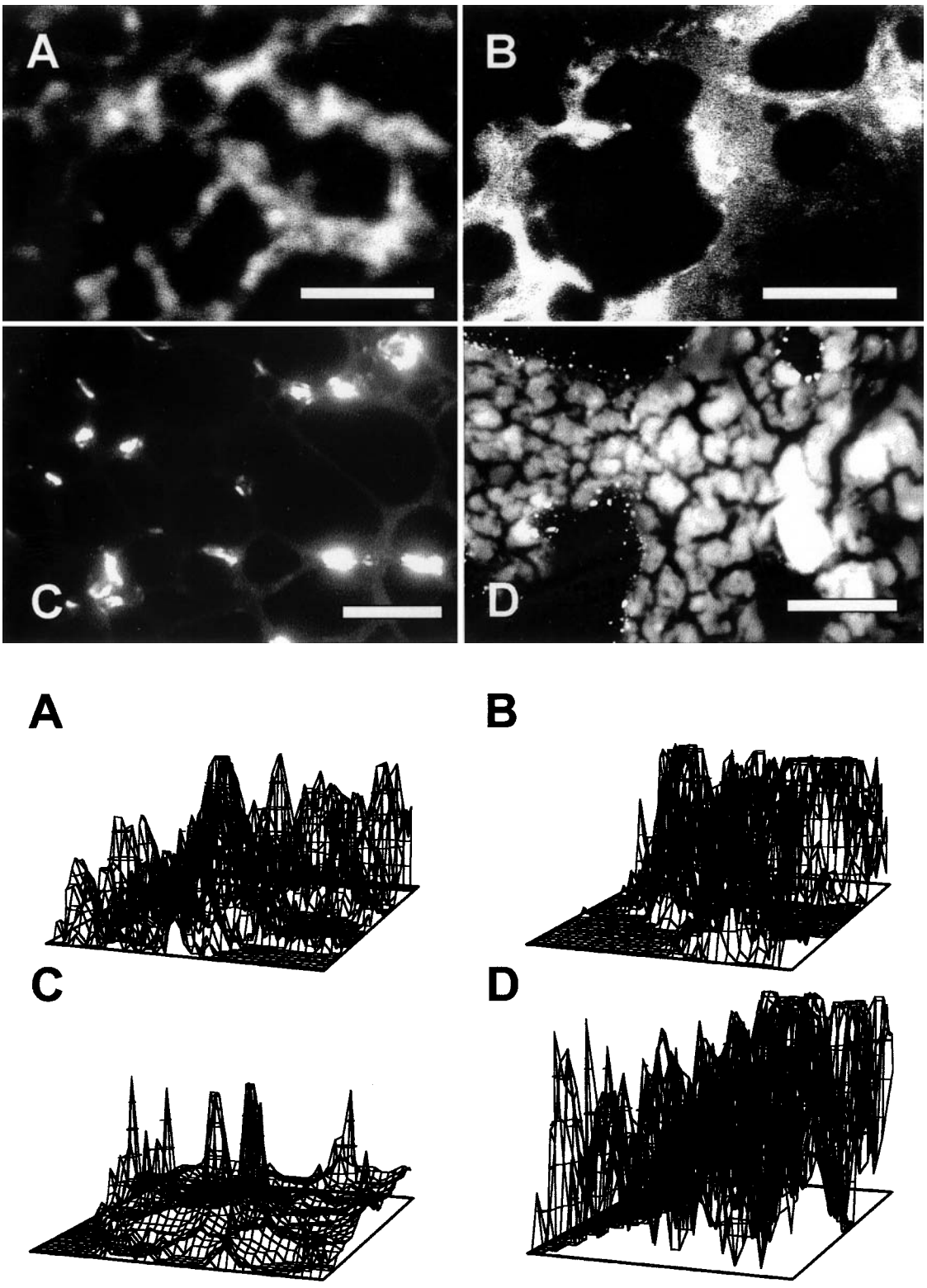

Fig. 3. Typical fluorescent microscope images (upper panel) and distribution of fluorescent intensity (bottom panel) of tumors from animals treated by P-FITC (A), P-TR (B), free DOX (C), and P(GFLG)-DOX (D). Scale bars indicate 50 μm. On the bottom panel the ordinate represents the average fluorescent intensity (from 10 adjacent pixels) in arbitrary units for corresponding picture from the upper panel.

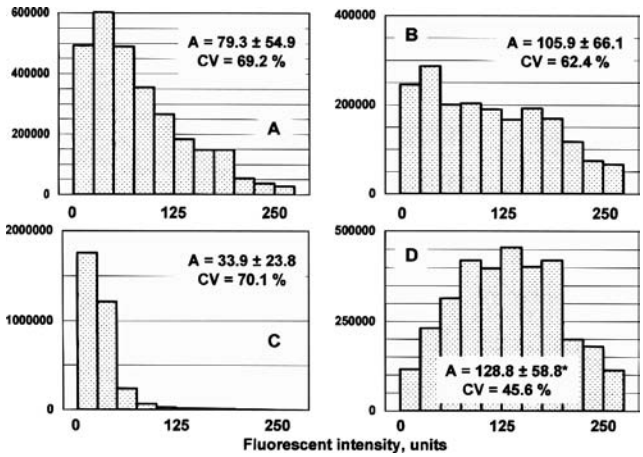

Fig. 4. Histograms of fluorescent intensity distribution measured for 30 slices of tumors treated by P-FITC (A), P-TR (B), free DOX (C), and P(GFLG)-DOX (D). Inserts show the average intensity (A, mean ± SD) and coefficient of variation (CV) calculated for the whole tumor. Ordinate represents the number of pixels, abscissa—fluorescent intensity in arbitrary units. The width of the bars (sample interval) equals to 25 units. $*P < 0.001$ when compared to free DOX.

study this component of the EPR effect we measured the expression of the *VEGF* gene by RT-PCR in different parts of the tumor (Fig. 6C). We registered the expression of two isoforms of the gene, which encode VEGF189 and VEGF121 proteins represented by 397 and 193 bp RT-PCR products, respectively. In all cases the *VEGF* gene was expressed more at the surface and less in the central parts of the tumor. P-FITC and P-TR did not change significantly the *VEGF* gene expression (data not shown). Treatment with free DOX resulted in the overexpression the *VEGF* gene in all parts of the tumor, while P(GFLG)-DOX led to the overexpression of the gene only at the exterior part of the tumor. Moreover, after the treatment P(GFLG)-DOX, we did not register the expression of the gene in the central core part of the tumor.

Apoptosis and Necrosis Detection

Two methods of cell death detection based on DNA fragmentation–DNA electrophoresis and detection of the mono- and oligonucleosomes by ELISA gave similar results (Fig. 7A, B). It was found that P-FITC and P-TR did not induce DNA fragmentation and cell death. In contrast to our previous data in DOX sensitive tumor (4), where we observed highly distinguished ladder-type of DNA fragmentation (characteristics of apoptosis), in the present study on DOX resistant tumors, the DNA fragmentation was less pronounced after treatment with free DOX and did not permit to distinguish between apoptotic and necrotic cell death. In contrast, P(GFLG)-DOX induced necrotic random DNA fragmentation which exceeded more than 6-times the control. These data confirm the high antitumor activity of P(GFLG)-DOX and seem to indicate that the main mechanism of cell death after the action of HPMA copolymer-bound DOX was necrosis. However, to determine the exact mode of cell death, other criteria like cellular morphology have to be considered; this will be the aim of our future studies.

DISCUSSION

The present study revealed that the *in vivo* antitumor activity of P(GFLG)-DOX was up to seven times higher when compared to free DOX. However, our previous *in vitro* study indicated that intracellular toxicity of P(GFLG)-DOX for the human ovarian carcinoma A2780/AD DOX resistant cells was only 2–3 times higher than free drug (3). This discrepancy may be explained in part by the specific distribution of the P(GFLG)-DOX within the organs. We revealed that it accumulated mainly in tumor tissue with only minor amounts found in other organs (4). In contrast, free DOX distributed widely trough the organs including liver, lung, spleen and heart. We also found that the distribution of HPMA copolymer-bound DOX in tumors significantly differed from the distribution of free DOX.

It is now well accepted that EPR effect is the predominant mechanism by which soluble macromolecular anticancer drugs exhibit their therapeutic effect on solid tumors (5–7). The phenomenon is attributed to high vascular density of the tumor, increased permeability of tumor vessels, defective tumor vasculature, and defective or suppressed lymphatic drainage in the tumor interstitium (7). A number of studies showed increased accumulation of macromolecules in tumors as compared to that in normal tissue (4–6,7,17). The degree of accumulation was dependent on molecular weight (7), charge (18,19) and their overall hydrophobic-hydrophilic character. The tumor type and microenvironment may influence its transport characteristics (pore cutoff size) (20). In addition to tumors, the EPR effect was also observed at sites of inflammation (21). However, our preliminary data (4) seem to suggest that the differences in tumor morphology after exposure to inert or cytotoxic macromolecules may dramatically influence the intratumor distribution of macromolecules. This may have an important impact on the EPR effect with concomitant changes in the therapeutic efficacy. To evaluate the relationship between the cytotoxicity of macromolecules on one hand and the tumor tissue morphology and drug efficacy on the other hand, we synthesized three HPMA copolymer conjugates. The first conjugate contained cytotoxic DOX, the others contained inert fluorophores FITC or Texas Red.

To avoid the influence of molecular weight on the EPR effect, we tried to keep the molecular weight of all conjugates very close (24–30 kDa). The molecular weight of the P(GFLG)-DOX and P-FITC was controlled by the amount of monomeric active ester in the feed polymerization mixture in the first step of the synthesis (p-nitrophenyl esters are known to decrease the M_w and polydispersity of polymers). The molecular weight of the polymer precursor containing amino groups (used for binding of Texas Red) was controlled by the addition of a chain transfer agent during polymerization (22).

Positively charged polymers are known to be rapidly eliminated from the blood circulation via urinary excretion or hepatic uptake (18), thus decreasing the chance for effective accumulation in the tumor. Therefore we have modified the residual amino groups (3.8 mol%) in side-chains of HPMA copolymer-bound Texas Red (P-TR) into carboxylic groups by reaction with succinic anhydride. It was shown before that neutral and slightly anionic macromolecules will have prolonged retention in the plasma circulation followed by large accumulation in the tumor (23). The fluorophores used exhibit a certain degree of hydrophobicity (FITC is less hydrophobic than TR). However,

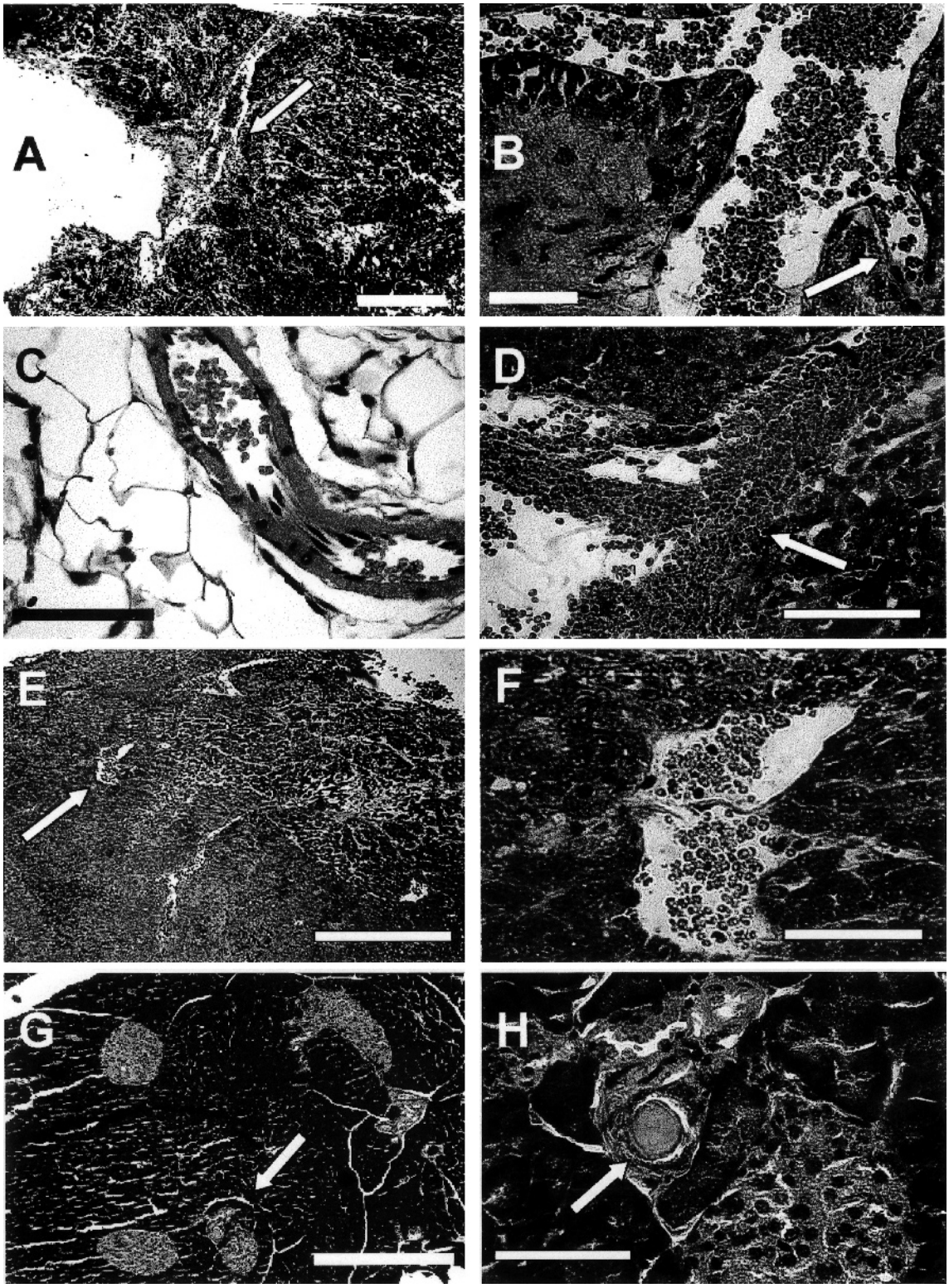

Fig. 5. Typical image of the control tumor (A, B) and tumors treated with free DOX (C, D), P-TR (E, F), and P(GFLG)-DOX (G, H) stained by hematoxylin-eosin. Scale bars represent 200 μm (A), 20 μm (B), 50 μm (C, D, F, H), and 500 μm (E, G), respectively. Arrows in A, E, G indicate the regions shown at a 10-times higher magnification on B, F, H, respectively. Arrows in B, D, H indicate irregularities in the microvessels described in detail in the text.

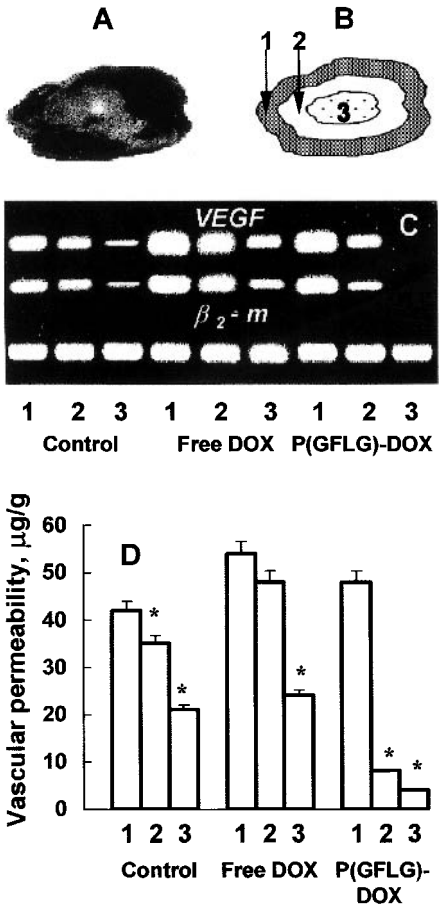

Fig. 6. *VEGF* gene expression and vascular permeability measured on the 32nd day of the experiments. Tumor (A) was excised and divided into 3 parts (B): 1–exterior highly vascularized part, 2–intermediate and 3–central core parts. The gene expression was measured by RT-PCR in each section (C, typical picture of RT-PCR products in agarose gel stained by ethidium bromide). Two isoforms of the *VEGF* gene encoded VEGF189 (397 bp) and VGF121 (193 bp) proteins were detected. The β_2-microglobulin (β_2-*m*) was used as internal standard. Vascular permeability was estimated by the amount of Evans Blue dye extracted from each section (D, means + SD from 4 independent measurements are shown). $*P < 0.05$ when compare to exterior part (1).

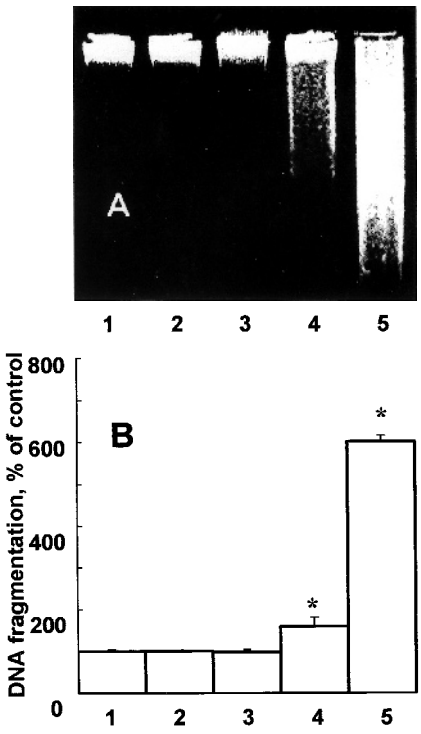

Fig. 7. DNA fragmentation measured by gel electrophoresis (A) and Cell Death ELISA (B). DNA was isolated from the tumor tissue and electrophoresed in 1% agarose gel and stained with ethidium bromide as described in the material and methods section (A). Figure B shows mean values + SD from 3 independent measurements of mono- and oligonucleosomal DNA fragments by ELISA as described. $*P < 0.05$ when compared to control. Tumor from animals on day 32 treated 6 times with: 1–no treatment (control); 2–P-FITC; 3–P-TR; 4–free DOX; 5–P(GFLG)-DOX.

due to their low content in HPMA copolymer conjugates (4–8 wt.%) the overall hydrophilic character of the polymer macromolecule was not substantially influenced (there was no sign of aggregation in the SEC profiles of the conjugates in PBS buffer).

As expected, all fluorescent HPMA copolymers—P-FITC, P-TR, and P(GFLG)-DOX—accumulated mainly in the tumor. However, inside the tumor, the distributions of HPMA copolymers which did not contain the drug (P-FITC, P-TR) and that with the drug (P(GFLG)-DOX) were substantially different. Although the distributions of P-FITC and P-TR were more homogenous when compared to free DOX, it preserved many features of that for free low molecular weight DOX. Namely, histograms of the distribution of P-FITC, P-TR and free DOX were characterized by significant shifts toward low concentrations (intensity of fluorescence) with long tails in the direction to higher concentrations (fluorescence). It appears that the majority of the tumor had a relatively low concentration of free DOX and or P-FITC or P-TR, while a high concentration was registered sporadically in some spots with apparently enhanced permeability. Analyzing the mechanisms of this type of distribution, one can assume that the highest concentrations of free DOX should be observed in tumor locations with the highest vascular permeability. This conclusion is supported by the data obtained by Sowter *et al.* (24), who found inhomogeneous distribution of the vascular permeability factor (vascular endothelial growth factor) expression in ovarian serous carcinoma very similar to the distribution of free DOX in our study. Vascular endothelial growth factor (VEGF), also known as vascular permeability factor, is a heparin-binding, dimeric polypeptide originally purified of its vascular permeability enhancing activity (25). VEGF is expressed in normal primate and human ovaries (26), and its expression is elevated in many human tumors, including ovarian carcinomas, as compared with normal tissues (27,28). It appears that an overexpression of the *VEGF* gene is one of the most important factors responsible for the EPR effect in tumors; however, other factors as bradykinin, nitric oxide, and peroxynitrate are involved (29). Analysis of gene expression in the present study showed that free DOX increased *VEGF* gene expression and vascular permeability in all parts of the tumor, even in its intermediate and central core parts. This might form a positive feedback loop when free DOX accumulates in the tumor locations with already high vascular permeability further increase the permeability and enhancing its accumulation, which in turn might increase the permeability,

etc. This positive feedback could lead to the highly inhomogeneous accumulation of free DOX in the tumor and decrease its antitumor activity. Data obtained in the present study seem to support the hypothesis. As it was first revealed in the present study, after repeated treatment of solid tumor by free DOX, the later accumulated in few limited regions of the tumor possessing high vascular permeability. The fluorescence (and probably concentration) of the drug in these spots at the end of the treatment was several orders of magnitude higher than in the other parts of the tumor (see Figs. 3 and 4). Consequently, DOX accumulated not only in the nucleus, but also in cytoplasm and intercellular space. This in turn led to the appearance of bright spots of fluorescence possessing a size significantly exceeding the size of nucleus. The hypothesis is also supported by the data obtained by Lankelma *et al.* (30), who revealed doxorubicin gradients in tumor islets in patients with breast cancer.

Different data were found when the tumor was treated with HPMA copolymer-bound DOX. In contrast to free DOX, P(GFLG)-DOX up-regulated the *VEGF* gene and increased tumor vascular permeability only in the exterior (growing) part of the tumor. It decreased both the *VEGF* expression and the permeability in the central necrotic parts of the tumor. This led to at least two main consequences. First, it enhanced the drug delivery to the living and progressively growing parts of the tumor. Second, it prevented the additional accumulation of the drug in already dead necrotic regions of the tumor. The combination of these factors finally led to the homogeneous distribution of the DOX within the tumor and to the augmentation of its anticancer activity.

CONCLUSIONS

1. The EPR effect is significantly different for macromolecules, which contain cytotoxic drug when compared to macromolecules with low cytotoxicity.

2. The cytotoxicity of polymer-drug conjugates amplifies the EPR effect, leads to a more homogenous distribution of the drug within the tumor, increases the average drug concentration in tumor and augments the efficacy of macromolecular drugs.

3. The accumulation of free DOX leads to the overexpression of the *VEGF* gene and increase of the vascular permeability in the spot of accumulation, which in turn enhances the drug accumulation at the same location. This forms a positive feedback loop, which probably leads to the highly inhomogeneous distribution of the drug within the tumor and decreases its antitumor effect.

4. In contrast, the accumulation of a significant amount of P(GFLG)-DOX in the tumor down-regulated the *VEGF* gene and decreased vascular permeability at the point of accumulation. This forms a negative feedback, which prevents additional drug accumulation in already dead necrotic tissue, resulting in a more uniform distribution and enhancement of the antitumor activity of HPMA copolymer-bound DOX.

ACKNOWLEDGMENTS

We thank Dr. A Suarato (Pharmacia-Upjohn, Milano, Italy) for the generous gift of doxorubicin. This research was supported in part by NIH grant CA 51578 from the National Cancer Institute.

REFERENCES

1. T. Minko, P. Kopečková, V. Pozharov, and J. Kopeček. HPMA copolymer bound adriamycin overcomes *MDR1* gene encoded resistance in a human ovarian carcinoma cell line. *J. Contr. Rel.* **54**:223–233 (1998).
2. T. Minko, P. Kopečková, and J. Kopeček. Chronic exposure to HPMA copolymer-bound adriamycin does not induce multidrug resistance in a human ovarian carcinoma cell line. *J. Contr. Rel.* **59**:133–148 (1999).
3. T. Minko, P. Kopečková, and J. Kopeček. Comparison of the anticancer effect of free and HPMA copolymer-bound adriamycin in human ovarian carcinoma calls. *Pharm. Res.* **16**:986–996 (1999).
4. T. Minko, P. Kopečková, and J. Kopeček. Efficacy of the chemotherapeutic action of HPMA coppolymer bound doxorubicin in a solid tumor model of ovarian carcinoma. *Int. J. Cancer,* **86**:108–117 (2000).
5. Y. Matsumura and H. Maeda. A new concept for macromolecular therapeutics in cancer chemotherapy: Mechanism of tumoritropic accumulation of proteins and the antitumor agent SMANCS. *Cancer Res.* **46**:6387–6392 (1986).
6. H. Maeda, L. M. Seymour, and Y. Miyamoto. Conjugates of anticancer agents and polymers: advantages of macromolecular therapeutics in vivo. *Bioconjugate Chem.* **3**:351–362 (1992).
7. Y. Noguchi, J. Wu, R. Duncan, J. Strohalm, K. Ulbrich, T. Akaike, and H. Maeda. Early phase tumor accumulation of macromolecules: A great difference in clearance rate between tumor and normal tissues. *Jpn. J. Cancer Res.* **89**:307–314 (1998).
8. J. Kopeček, P. Rejmanová, J. Strohalm, K. Ulbrich, B. Říhová, V. Chytrý, J. B. Lloyd, and R. Duncan. Synthetic polymeric drugs. U.S. Pat. 5,037,883 (Aug. 6, 1991).
9. V. G. Omelyanenko, P. Kopečová, C. Gentry, J.-G. Shiah, and J. Kopeček. HPMA copolymer-anticancer drug-OV-TL16 antibody conjugates. 1. Influence of the methods of synthesis on the binding affinity to OVCAR-3 ovarian carcinoma cells in vitro. *J. Drug Target.* **3**:357–373 (1996).
10. V. Omelyanenko, P. Kopečková, C. Gentry, and J. Kopeček. Targetable HPMA copolymer-adriamycin conjugates. Recognition, internalization, and subcellular fate. *J. Contr. Rel.* **53**:25–37 (1998).
11. E. Tischler, R. Mitchell, T. Hartman, M. Silva, D. Gospodarowicz, J. C. Fiddes, and J. A. Abraham. The human gene for vascular endothelial growth factor: Multiple protein forms are encoded through alternative exon aplicing. *J. Biol. Chem.* **266**:11947–11954 (1991).
12. B. C. Trauth, C. Klas, A. M. Peters, S. Matzku, P. Moller, W. Falk, K. M. Debatin, and P. H. Krammer. Monoclonal antibody—mediated tumor regression by induction of apoptosis. *Science.* **245**:301–305 (1989).
13. H. F. Dvorak, J. A. Nagy, J. T. Dvorak, and A. M. Dvorak. Identification and characterization of the blood vessels of solid tumors that are leaky to circulating macromolecules. *Am. J. Pathol.* **133**:95–109 (1988).
14. F. Yuan, M. Dellian, D. Fukumura, M. Leuning, D. A. Berk, V. P. Torchilin, and R. K. Jain. Vascular permeability in a human tumor xenograft: molecular size dependence and cutoff size. *Cancer Res.* **55**:3752–3756 (1995).
15. L. E. Benjamin, R. Goljanin, A. Irin, D. Pode, and E. Keshet. Selective ablation of immature blood vessels in established human tumors follows vascular endothelial growth factor withdrawal. *J. Clin. Invest.* **103**:159–165 (1999).
16. S. Mesiano, N. Ferrara, and R. B. Jaffe. Role of vascular endothelial growth factor in ovarian cancer. *Am. J. Pathol.* **153**:1249–1256 (1998).
17. J.-G. Shiah, Y. Sun, C. M. Peterson, and J. Kopeček. Biodistribution of free and N-(2-hydroxypropyl)methacrylamide copolymer-bound mesochlorin e_6 and adriamycin in nude mice bearing human ovarian carcinoma OVCAR-3 xenografts. *J. Contr. Rel.* **61**:145–157 (1999).
18. Y. Tabata, T. Kawai, Y. Murakami, and Y. Ikada. Electric charge influence of dextran derivatives on their tumor accumulation after intravenous injection. *Drug Delivery* **4**:213–221 (1997).
19. S. K. Hobbs, W. L. Monsky, F. Yuan, W. G. Roberts, L. Griffith,

V. P. Torchilin, and R. K. Jain. Regulation of transport pathways in tumor vessels: Role of tumor type and microenvironment. *Proc. Natl. Acad. Sci.* USA **95**:4607–4612 (1998).
20. Y. Murakami, Y. Tabata, and Y. Ikada, Effect of the molecular weight of water-soluble polymers on accumulation at an inflammatory site following intravenous injection. *Drug Delivery* **3**: 231–238 (1996).
21. Z-R. Lu, P. Kopečková, Z. Wu, and J. Kopeček. Synthesis of semitelechelic poly[N-(2-hydroxypropyl)methacrylamide] by radical polymerization in the presence of alkyl mercaptans. *Macromol.Chem. Phys.* **200**:2022–2030 (1999).
22. Y. Takakura and M. Hashida. Macromolecular carrier systems for targeted drug delivery: pharmacokinetic consideration on biodistribution. *Pharm. Res.* **13**:820–831 (1996).
23. H. M. Sowter, A. N. Corps, A. L. Evans, D. E. Clark, D. S. Charnok-Jones, and S. K. Smith. Expression and localization of the vascular endothelial growth factor family in ovarian epithelial tumors. *Lab. Invest.* **77**:607–614 (1997).
24. N. Ferrara and W. J. Henzel. Pituitary follicular cells secrete a novel heparin-binding growth factor specific for vascular endothelial cells. *Biochem. Biophys. Res. Commun.* **161**:851–858 (1989).
25. N. Ravindranath, L. Little-Ihrig, H. S. Phillips, N. Ferrara, and A. J. Zeleznik. Vascular endothelial growth factor messenger ribonucleic acid expression in the primate ovary. *Endocrinology* **131**:254–260 (1992).
26. T. A. Olson, D. Mohanraj, L. F. Carson, and S. Ramakrishnan. Vascular permeability gene expression in normal and neoplastic human ovaries. *Cancer Res.* **54**:276–280 (1994).
27. D. R. Senger, C. A. Perruzzi, J. Feder, and H. F. Dvorak. A highly conserved vascular permeability factor secreted by a variety of human and rodent tumor cell lines. *Cancer Res.* **46**:5629–5632 (1986).
28. B. Berse, L. F. Brown, L. Van De Watter, A. Papadopoulos-Sergiou, C. A. Perruzzi, E. J. Manseau, H. F. Dvorak, and D. R. Senger. Vascular permeability factor (vascular endothelial growth factor) gene is expressed differentially in normal tissues, macrophages, and tumors. *Mol. Biol. Cell* **3**:211–220 (1992).
29. H. Maeda, J. Wu, S. Tamaka, and T. Akaike. Modulation of tumor vascular permeability and EPR effect for macromolecular therapeutics. In 9th *International Symposium on Recent Advances in Drug Delivery Systems*, February 22–25, 1999, Salt Lake City, USA, p. 114–117.
30. J. Lankelma, H. Dekker, R. F. Luque, S. Luykx, K. Hoekman, P. van der Valk, P. J. van Diest, and H. M. Pinedo. Doxorubicin gradients in human breast cancer. *Clin. Cancer Res.* **5:**1703–1707 (1999).